Stretchable Wireless System for Sweat pH Monitoring

Wenting Dang[1], Libu Manjakkal[1], William Taube Navaraj[1], Leandro Lorenzelli[2], Vincenzo Vinciguerra[3] and Ravinder Dahiya[1]*

[1]Bendable Electronics and Sensing Technologies (BEST) group, School of Engineering University of Glasgow, UK

[2]Microsystems Division, Fondazione Bruno Kessler, Trento. 38123, Italy

[3]ST Microelectronics, Catania, Italy

Correspondence to: Ravinder.Dahiya@glasgow.ac.uk

Abstract

Sensor-laden wearable systems that are capable of providing continuous measurement of key physiological parameters coupled with data storage, drug delivery and feedback therapy have attracted huge interest. Here we report a stretchable wireless system for sweat pH monitoring, which is able to withstand up to 53% uniaxial strain and more than 500 cycles to 30% strain. The stretchability of the pH sensor patch is provided by a pair of serpentine-shaped stretchable interconnects. The pH sensing electrode is made of graphite-polyurethane composite, which is suitable for biosensor application. The sensing patch validated through in-depth electrochemical studies, exhibits a pH sensitivity of 11.13±5.8 mV/pH with a maximum response time of 8 s. Interference study of ions and analyte (Na^+, K^+ and glucose) in test solutions shows negligible influence on the pH sensor performance. The pH data can be wirelessly and continuously transmitted to smartphone through a stretchable radio-frequency-identification antenna, of which the radiating performance is stable under 20% strain, as proved by vector network analyzer measurement. To evaluate the full system, the pH value of a human sweat equivalent solution has been measured and wirelessly transmitted to a custom-developed smart phone App.

Keywords: stretchable pH sensor; stretchable antenna; wireless system; sweat analysis, health monitoring

1. Introduction

Recent technological advances in the field of flexible electronics and wireless communication have fueled a new wave in the healthcare sector by enabling non-invasive methods for continuous monitoring of key physiological parameters such as heart rate, blood pressure, skin temperature, electrocardiogram and respiration rate (Dahiya, 2015; Farandos *et al.*, 2015; Gao *et al.*, 2016; Imani *et al.*, 2016; Lee *et al.*, 2017; Liu *et al.*, 2017; Takei *et al.*, 2015; Gupta *et al.*, 2018). Wearable systems based on these technological advances underpin the shift in the healthcare paradigm towards individual centric management of health, also known as mobile health (mHealth) (Quesada-González and Merkoçi, 2017) self-health management (Haghi *et al.*, 2017). The electronics on flexible and stretchable substrates allows wearable systems to conform to body parts and thus improves the reliability of non-invasive data collection. Non-invasive systems for diagnosis and health monitoring (particularly for chronic ailments) will have a major impact on healthcare practices as patients are likely to be more compliant with such methods (World Health Organization, 2011). These methods are also attracting a lot of attention because of ease of use. In addition, such systems can be used in low-resource settings without the need for highly trained medical staff, and have the potential to greatly improve patient care in disease outbreaks where complex sample handling is undesirable. For this reason, recently there has

Table 1 Analytes in blood, tears and sweat with their diagnostic significance (Corrie *et al.,* 2015; Farandos *et al.,* 2015; Tinku *et al.,* 2014).

Analytes	**Blood (mM)**	**Tear (mM)**	**Sweat(mM)**	**Diagnostic application**
Glucose	3.3-6.5	0.013-0.051	0.33-0.65	Hyper/hypo Glycaemia /Diabetes
Lactate	3.6-7.5	1.1-2.1	13.4-26.7	Ischemia, Sepsis, Liver disease, Cancer
Urea	6.2±0.9	3.0-6.0	22.2±8.0	Uraemia indicating Renal dysfunction
Creatinine	0.077-0.127	0.014-0.051	0.014-0.051	Renal dysfunction
Na^+	140.5±2.2	120–165	66.3±46.0	Hyper/hyponatremia
K^+	4.8±0.8	20–42	9.0±4.8	indicator of ocular disease
Ca^{2+}	2.0–2.6	0.4–1.1	4-60	Hyper/hypo Calcemia
Mg^{2+}	0.7–1.1	0.5–0.9	0.6	Acidosis and muscle contraction
Cl^-	98.9±6.7	118–135	59.4±30.4	Hyper/hypo Chloremia
Pyruvate	0.1–0.2	0.05–0.35	0.003- 1	Disorders of energy metabolism
Ascorbate	0.04–0.06	0.22–1.31	0.43	Diabetes

been increased interest in monitoring health conditions through body fluids such as sweat, tears and urine etc. (Farandos *et al.*, 2015; Gao *et al.*, 2016; Lee *et al.*, 2017).

As depicted in Table 1, various analytes such as glucose, urea, ascorbate are found in both the blood as well in tear and sweat and research suggests that there is a correlation among them. These body fluids could be potential treasure trove for diagnosing several diseases (including chronic diseases) and might eliminate the need for acquiring blood samples. Sweat is particularly attractive as it is readily available and is strongly correlated to the blood (Heikenfeld, 2014; Sakharov *et al.*, 2010) (Table 1). By measuring some of these analytes in the sweat, it is possible to diagnose diseases such as diabetes, hypocalcemia, hypochloremia etc. The pH determination is essential in sweat monitoring as it can reflect the variations in the concentration of various electrolytes in sweat that can indicate disease and metabolic activity (Patterson *et al.*, 2000; Sonner *et al.*, 2015). As an example, the pH value of healthy person is in the range of 4.5-6.5, but patients with cystic fibrosis have alkaline sweat (up to pH 9) due to the defect in bicarbonate-reabsorption (H^+-secretion) (Nikolajek and Emrich, 1976). The pH value in sweat is also an indicator for the human body's exercise intensity and dehydration level. While exercising, the concentration of ammonia in sweat decreases due to its transformation into ammonium (NH_4^+). As NH_4^+ is less diffusible across cellular membranes compared to ammonia, the excess NH_4^+ molecules accumulate ions which leads to an increase in sweat pH (Czarnowski and Gorski, 1991; Sonner *et al.*, 2015). Considering these, the reliable monitoring of sweat pH is essential for health monitoring and wellness applications. This is a vital step towards realizing a multi-sensory conformable system for a comprehensive sweat-based health monitoring.

It is challenging to have a fully integrated wearable system (with data process and transmission modules) that could maintain a conformal physical contact with human skin, especially under dynamic motions (Bandodkar *et al.*, 2013; Lee *et al.*, 2017; Nakata *et al.*, 2017). Few methods explored to improve conformal contact include using ionogel as a sensitive layer (Curto *et al.*, 2012), adhesive stickers (Anastasova *et al.*, 2017; Huang *et al.*, 2014) and tattoo papers (Bandodkar *et al.*, 2013) etc. These sensing solutions are not stretchable and long-term wearing of stickers may cause irritation. Furthermore, it is difficult to realize a miniaturized and light-weight wearable system with integrated signal transmission circuitry, especially with non-flexible or rigid devices used for Bluetooth

technology (Anastasova *et al.*, 2017; Kim *et al.*, 2015; Liu *et al.*, 2016; Rose *et al.*, 2015). These reported solutions allow continuous wireless data transmission, but with bulky and rigid Bluetooth modules, which also consume significant energy and require frequent charging. This issue could be addressed with stretchable radio-frequency-identification (RFID) coils as demonstrated here in this paper.

The stretchable pH sensing system presented in this paper comprises of a stretchable pH sensor with stretchable RFID antenna and data processing and transmission circuitry to communicate with smartphone. Benchmarked in Table S1 and S2, the presented stretchable pH sensing and communicating system has several advantages in terms of fast sensing response, mechanical robustness and real-time data transmission under dynamic motion. The sensing electrodes of pH sensor are based on graphite-polyurethane composite. Compared with materials such as metal oxide used for pH sensing (Anastasova *et al.*, 2017; Manjakkal *et al.*, 2014; Nakata *et al.*, 2017; Simić *et al.*, 2017), the graphite-polyurethane composite is advantageous in terms of flexibility and fast response. These composites exhibit excellent performance in bio-sensing application especially for determining dopamine, epinephrine, furosemide etc. (Baccarin *et al.*, 2018; de Toledo *et al.*, 2005; Saciloto *et al.*, 2013; Semaan *et al.*, 2008). One of the major advantages of these composite is their processing at low temperatures (80°C), which are compatible with conformable substrate. In this work, we have reported for the first time the use of graphite-polyurethane composite as a pH sensitive electrode together with Ag/AgCl paste as a reference electrode forming a potentiometric pH sensor for sweat analysis. In the majority of reported biosensors based on graphite-polyurethane composite, the sensing mechanism was based on electrochemical oxidation reaction between analytes and composite. In this work we have utilized the electrical double layer (EDL) formation between the graphite-polyurethane composite electrode and pH solution. The pH sensing electrode (SE) and the printed Ag/AgCl quasi-reference electrode (RE) are connected through stretchable interconnects to allow the pH sensor to withstand up to 53% strain without compromising their electrical performance. As human skin experiences an average strain of 30% (Matsuhisa *et al.*, 2015), the stretchable pH sensing patch presented here can be conformably attached to the skin and used with minimal influence on their electrical performance. To demonstrate the wireless

data transmission, the pH sensor patch is integrated with a stretchable antenna. The full stretchable wireless pH sensing system is shown in Fig. 1(a).

2. Material and Methods

2.1. pH sensor design and fabrication

The pH sensor comprises of a pair of stretchable interconnects, and graphite-polyurethane composite together with Ag/AgCl reference electrode as a potentiometric sensing structure as illustrated in Fig. 1(b). The optimization of the composite was carried out in terms of trade-off between printability and the conductance of graphite-polyurethane composite electrode. Fig. S9 shows the typical resistance vs frequency characteristics of 1:1 and 1:2 graphite-polyurethane composites. Higher polyurethane concentration renders the composite non-conducting. Higher graphite concentration results in higher conductivity while resulting in poor printability of the composite due to lack of adhesion. A 1:1 ratio of graphite-polyurethane was found to be suitable for this application which was extensively characterized using impedance, capacitance and potentiometric analysis as explained in Section 3.1. The optimal geometry of stretchable interconnects (serpentine shape with 260º arc curvature, obtained with electro-mechanical studies in COMSOL) used here provides the maximum stretchability to the pH sensors (Appendix B). The graphite-polyurethane composite based pH SE and Ag/AgCl RE are deposited on the contact pad (1×1 mm^2) of interconnects (500 µm width). The overall sensor is encapsulated in the polydimethylsiloxane (PDMS).

The detailed fabrication process of stretchable interconnects is illustrated in Fig. 1(c). Firstly, the polyimide (PI) (DuPont) was spun on 100 nm-thick poly(methyl methacrylate) (PMMA) (Sigma Aldrich) coated silicon wafer at the spin rate of 3000 rpm for 30s. Curing for three hours at 200°C in nitrogen ambient resulted in the PI film with 7 µm thickness (confirmed by interferometer (Leitz Ergolux) measurement). Then, a stack of Cr/Au (5/150 nm) metal was electron beam (e-beam) evaporated and this was followed by a brief (15s at 200W) oxygen plasma treatment on PI film. In the next step, a 10-µm-thick positive photoresist was used with bright field mask. During UV exposure and development processes, the designed pattern protects the metal stack from wet etching and the PI film from dry etching. The interconnects fabricated on silicon wafer were then transferred to PDMS substrate

by using water soluble tape (3M, US), as shown in Fig. 1(c)(I-IV). The PDMS substrate (180 µm thick) was obtained separately by spin coating a 10:1 (base polymer: crosslink) the solution on silanized silicon wafer at 300 rpm for 60 s and curing in the oven for 2 hours at 80°C.

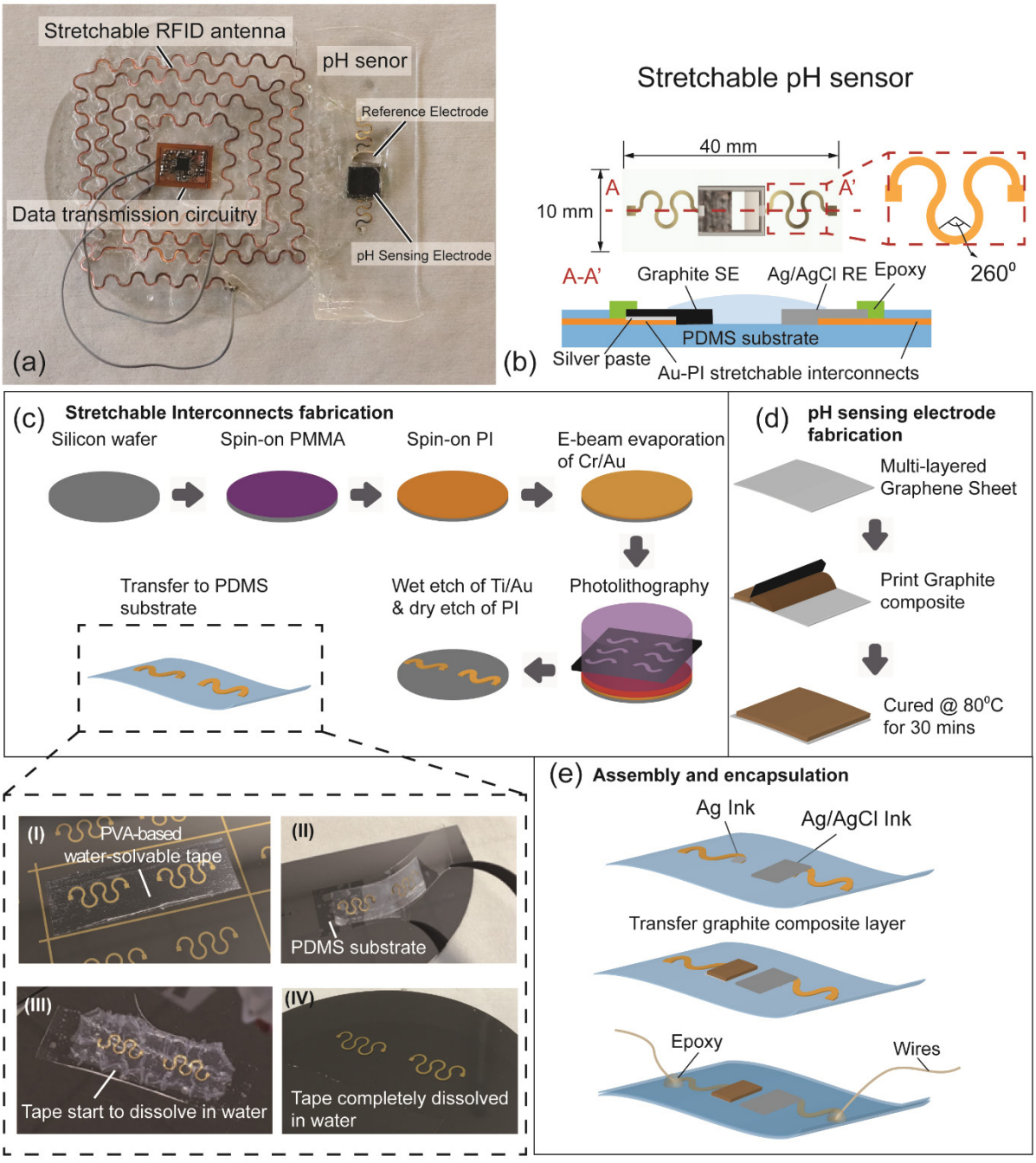

Fig. 1. (a) Photo of stretchable wireless system for sweat pH monitoring, (b) Schematic diagram of stretchable pH sensor with graphite-polyurethane composite SE, Ag/AgCl-based RE and a pair of

stretchable interconnects. Schematic diagram of the fabrication process for (c) stretchable interconnects, (d) SE electrodes (e) assembly and encapsulation of sensor patch.

For each pH sensor, a pair of stretchable interconnects were prior transferred to PDMS substrate. The pH SE was fabricated by printing graphite-polyurethane composite (1:1 ratio) paste on the top of multi-layered graphene sheet (Graphene Supermarket, US), which accelerate the electron transportation during ion exchange between SE and solution. The electrode was then cured in oven at 80°C for 30 mins. The fabrication procedure of pH SE is shown in Fig. 1(d). After obtaining the pH SE, the SE and RE electrodes were assembled and encapsulated as shown in Fig. 1(e). The pH SE (8×8 mm^2) was connected to one of the stretchable interconnects by using conductive epoxy silver ink. The Ag/AgCl ink (Gwent Group, UK) was then drop casted to the contact pad from the second interconnect, which is used as RE in the sensor. To ensure a robust connection between SE/RE and stretchable interconnects, the epoxy glue was applied to the connection area. The epoxy glue also serves as a barrier during drop casting of top encapsulation PDMS layer to allow the sensing area to contact with solution under test.

2.2. Stretchable antenna design and fabrication

The stretchable RFID antenna developed here is effective for Near Field Communication (NFC), which requires 13.56 MHz resonant frequency. The antenna is designed to have inductance together with the capacitors and the internal capacitance to match with the RFID transponder IC (TI RF430FRL152H), used here as interface between the sensor and the antenna coil (Fig. 2(a)). The specification of the transponder IC requires a 1.84 μH inductance. The designed square-shaped spiral coil antenna has inductance of 1.88 μH. This value was estimated through a modified wheelers equation (Mohan *et al.*, 1999):

$$L = \frac{\mu n^2 d_{avg} C_1}{2}\left(\ln\left(\frac{C_2}{\rho}\right) + C_3\rho + C_4\rho^2\right) \quad (1)$$

Where, μ refers to the vacuum permittivity ($4\pi\times10^{-7}$ H/m), n is the number of turns in the loop, d_{avg} is the average diameter of antenna ($d_{avg} = \frac{d_{out}+d_{in}}{2}$), ρ is the fill ratio ($\rho = \frac{d_{out}-d_{in}}{d_{out}+d_{in}}$) and the C_i are the coefficient based parameters. The square-shaped antenna has 4 turns with the turn width of 1 mm and 1 mm spacing between adjacent turns. The outer/inner dimension of antenna is 6/4.6 mm. The

antenna design was further modified to obtain wavy or serpentine shaped coils as shown in the inset of Fig. 2(b). The inner/outer radius of wavy structure is 1.5/2.5 mm with an arc degree of 180º. The minimum space between each turn of the coil is 1 mm. To estimate the influence of stretching on antenna's output, an approximate estimation was performed using basic magnetic flux and self-inductance equations (Eq. S1-2, Appendix C). The induced magnetic flux is strongly related to the area enclosed by coil. The maximum strain which the antenna can withstand (calculated from the length of stretchable antenna) is about 40%. For a square-shaped in-plane coil, the influence of stretching on the area A was estimated by using equation $A'/A = (1+\varepsilon)\cdot(1-\nu\varepsilon)$. Here A' is the enclosed area after stretching, ε is the external strain introduced during stretching and ν is the Poisson's ratio. Considering the Poisson's ratio is 0.34 (for copper) and 0.4 as strain, the area will increase 20%. Based on Eq. S3-4, the Q factor will change by 4%.

To obtain the designed antenna, a rapid prototyping method with blade cutters (Silhouette Cameo) was used to obtain the stretchable antenna. The cutting systems used here results in cut-width of about 50 µm (Garcia Núñez *et al.*, 2017). As compared with the standard microfabrication, this method is economical and faster. To obtain the antenna with high conductance, we used a flexible polyimide film with copper clad (Pyralux, DuPont) on one-side. The thickness of polyimide and copper films are 94 µm and 18 µm respectively. Prior to blade cutting, the water-soluble glue was applied to the copper sheet and the sheet was then laminated to the cutting mat (Fig. 2(i) and (d)). During blade cutting, the parameters such as blade speed, height and cutting thickness were adjusted to prevent the copper sheet from getting damaged (Fig. 2(ii)). Then rest of the material was carefully removed (Fig. 2(iii)). Afterwards, the patterned antenna structure was transferred to blue tape (dry photoresist) by dissolving the sacrificial water-soluble layer in the water (Fig. 2(iv-v) and (e)). In the following step, the patterned antenna on blue tape was adhered to partially cured PDMS substrate (spin-coated on silicon wafer and baked for 30 mins at 70°C). The blue tape was dissolved in acetone after the PDMS was fully cured (Fig. 2(vii) and (f)). At last, the stretchable antenna on PDMS substrate was detached from silicon wafer (Fig. 2(viii)). The inductance of fabricated antenna, measured by LCR meter (E4980AL, Keysight), was found to be 1.89 µH.

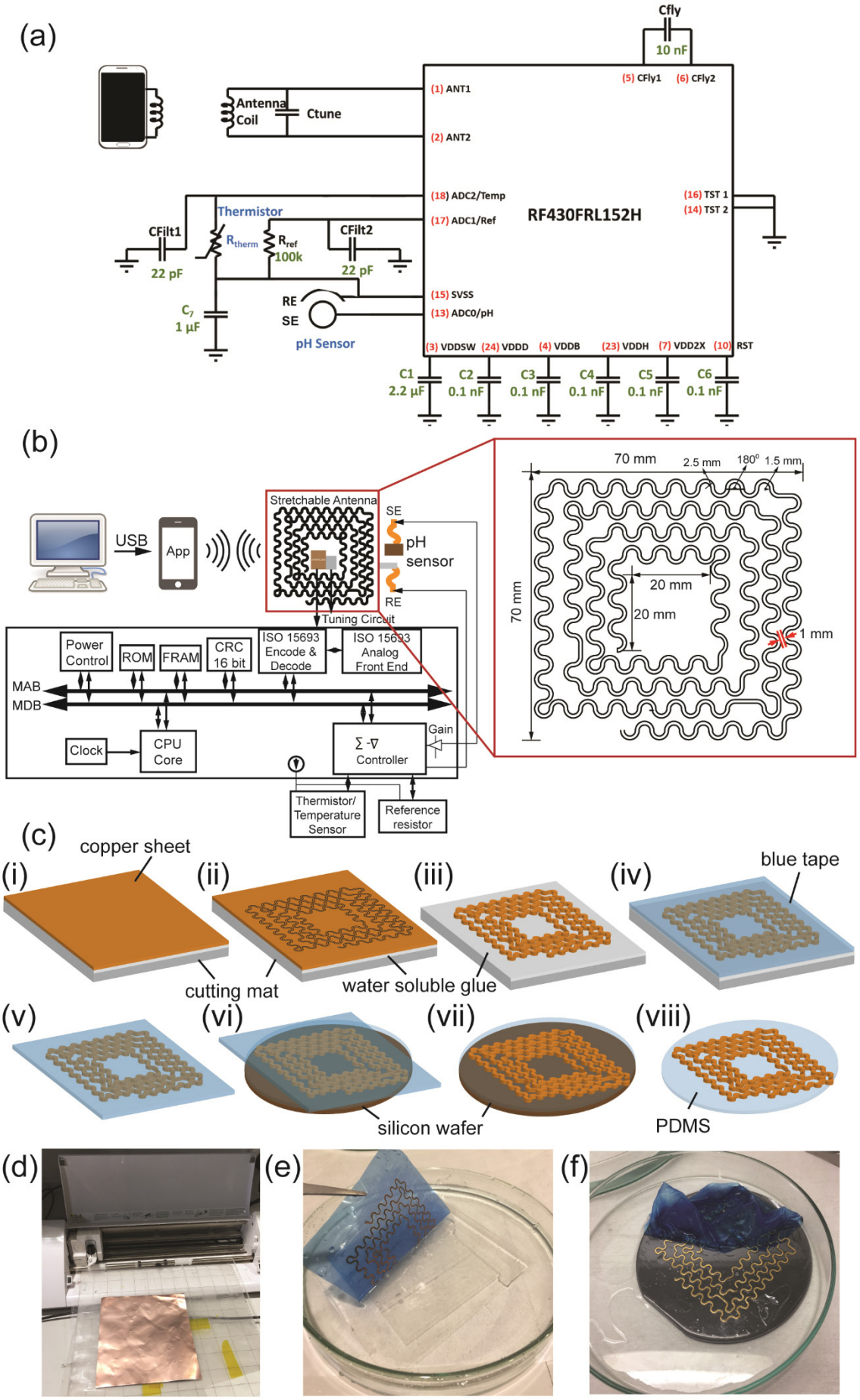
(a)
Cfly
10 nF
(5) CFly1
(6) CFly2
(1) ANT1
Antenna Coil
Ctune
(2) ANT2
(18) ADC2/Temp
(17) ADC1/Ref
RF430FRL152H
(16) TST 1
(14) TST 2
Thermistor
CFilt1
22 pF
Rtherm
Rref 100k
CFilt2
22 pF
(15) SVSS
(13) ADC0/pH
RE
SE
pH Sensor
C7 1 µF
(3) VDDSW
(24) VDDD
(4) VDDB
(23) VDDH
(7) VDD2X
(10) RST
C1 2.2 µF
C2 0.1 nF
C3 0.1 nF
C4 0.1 nF
C5 0.1 nF
C6 0.1 nF
(b)
USB
App
Stretchable Antenna
SE
pH sensor
RE
Tuning Circuit
Power Control
ROM
FRAM
CRC 16 bit
ISO 15693 Encode & Decode
ISO 15693 Analog Front End
MAB
MDB
Clock
CPU Core
Σ -∇ Controller
Gain
Thermistor/ Temperature Sensor
Reference resistor
70 mm
2.5 mm
180°
1.5 mm
70 mm
20 mm
20 mm
1 mm
(c)
copper sheet
(i)
(ii)
(iii)
(iv)
blue tape
cutting mat
water soluble glue
(v)
(vi)
(vii)
(viii)
silicon wafer
PDMS
(d)
(e)
(f)

Fig. 2. (a) Circuit design and (b) system-level block diagram for wireless pH data transmission with the inset image of antenna design and (c) Fabrication steps of stretchable antenna including (i) laminating flexible copper sheet to cutting mat with water-soluble glue as sacrificial layer, (ii) blade cutting the antenna pattern, (iii) removing the rest of material, (iv) attaching the blue tape over the antenna pattern, (v) dissolving the glue in water and transferring the antenna pattern to blue tape, (vi) adhering to partially cured PDMS substrate (separately prepared through spin-coating on silicon wafer), (vii) curing PDMS and dissolving blue tape in acetone and (viii) detaching the PDMS substrate from silicon wafer. Photos of critical steps c(i), c(v) and c(vii) are also included in (d), (e) and (f) respectively.

2.3. Wireless data transmission system

The circuit and system-level block diagram for the realized pH sensor and interface with NFC are shown in Fig. 2(a) and (b). The stretchable pH sensing patch uses TI RF430FRL152H RFID sensor transponder integrated circuit (IC) as an interface between the pH sensor and the smartphone readout app. The IC was also used to read the skin temperature with a thermistor (ERT-J1VS104FA) as a sensor. The stretchable antenna is connected to the ISO15693 RF analog frontend of RFID transponder IC with ANT1 and ANT2 pins. The design of stretchable antenna was discussed in previous section. The inductance (L) of the coil and tuning capacitors (C_{tune}) are used to tune the RFID frequency to 13.56 MHz as per the equation$f = 1/(2\pi\sqrt{(LC_{tune}}))$. The internal capacitance of IC is also considered in these calculations. The battery-free operation of sensor patch was achieved with electromagnetic energy harvesting circuitry of RF reader. In the two-electrode configuration, the sensor is electrochemically powered and does not require any external power for its operation. For a pH variation from 5 to 9, typically the pH sensor output between the two electrodes varies from 80 mV to 160 mV. The SE was connected to one of the analog to digital converter (ADC0) and the RE to SVSS. The internal configuration registers of the transponder IC were programmed through the same smartphone app to perform readout of the pH sensor and the thermistor. The thermistor (R_{therm}) was connected to ADC2 and a reference resistor (R_{ref}) was connected to ADC1. The other terminals were connected to SVSS. With the virtual ground option enabled, during ADC sampling the SVSS voltage is raised to approximately 125 mV above ground. This prevents minor errors that arise from the nonlinear behavior

of ADC closer to ground level. The blocks and functionality of ICs, explained here in context with pH sensor interface, are also applicable to other sensors and multi-sensor interface applications. The sensor transponder IC has a MSP430™ mixed-signal microcontroller as the core architecture, which is suitable for smart sensing and processing applications. Furthermore, it uses a Ferroelectric Random-Access Memory (FRAM) which is suitable for fast writing at low power. The core of IC communicates with other modules through Memory Address Bus (MAB) and Memory Data Bus (MDB). The commands and data are sent from the smartphone to RFID chip via ISO15693 analog front end, which are decoded by ISO15693 decode module (or encoding during transmission from RFID to the smartphone). The commands and the data are checked for error by the cyclic redundancy check (CRC) module. The firmware is stored in a ROM, which carries out the readout routine. For accurate measurement of temperature, a reference resistor was also used. The "UsingThermistor" bit of error control register was set and this results in an output current of ~2.4 μA on the ADC2 and ADC1 pins. The resistance of thermistor can be determined as: $R_{therm} = \frac{ADC2\ Net\ Result}{ADC1\ Net\ Result} \times R_{ref}$. The temperature is determined from the resistance value, which is based on the temperature coefficient of resistance. The temperature value can be used either as the monitoring parameter or to calibrate the pH sensor's output based on experimentally observed temperature dependence.

The calibration routine was also implemented in the smartphone app. The voltage level of a buffer solution with known pH value was used for performing the calibration. The relationship between voltage and pH of test solution was estimated based on calibration with standard buffer solution. The output of the pH sensor was read through the 14-bit ∑-Δ convertor. The ADC0, ADC1, ADC2 skip count register bits were programmed to sample every sampling time without any skip. To achieve sensing in the range of hundred mV, where the potentiometric pH sensor performs, the gain for the conversion of pH sensor read out was set according to the potentiometric characterization curve in sensor analysis section 3.1, to allow for the potential output from the sensor to the ADC module. The chip was configured to perform cascaded integrator–comb (CIC) filtering on the sampled data with a decimation ratio of 256 to achieve noise reduction. The pH sensor's value is measured with respect to V_{SS} ground. The low threshold/ high threshold alarm configurations register bits for both these sensors

were disabled. The device was configured to operate in Low Power Mode 3 (LPM3). The device was programmed to send data once in every 5 seconds, with a single pass readout for both sensors' measurements. During continuous readout, the status registers were checked for the sampling process to complete and for data availability. Then the data is read from the FRAM, and the ADC values and corresponding raw voltages are converted and displayed as pH and temperature values using pre-calibrated equations. The option of storing the data has been added to allow users to record the sweat pH for comparison and regular tracking. The users can view the stored history of data both in a daily interactive graph indicating the mean and range of pH for each day as shown in Figure S10a. And touch action on one of the daily data point shows a minute-by-minute interactive graph for any given day as shown in Figure S10b. The users can scroll around, pan, zoom in, zoom out of the displayed graph to understand the trend and perform comparison. The video of this feature is shown in supplementary video 3.

2.4. Reagent for pH sensor characterization

Three sets of testing solution were used for performance analysis of the fabricated sensors. These include: (1) pH buffer solution ranging from 5 to 9 (Sigma Aldrich); (2) Dulbecco's Modified Eagle Medium (DMEM, Sigma-Aldrich), which is a standard culture medium used for maintaining mammalian cell *in vitro*; and (3) solution equivalent of human sweat prepared by mixing NaCl (Sigma Aldrich), KCl (Sigma Aldrich) and lactic acid (Sigma Aldrich) in deionized water according to the concentration in Table 1. The pH value of DMEM was tuned by adding diluted HCl and KOH solutions. The pH measurement technique used for acquiring reference values in all comparison studies and for calibration were acquired by using a commercial digital pH tester HI 98130 from Hanna® Instruments fitted with a HI 73127 pH electrode except some samples in which case standard buffered pH solutions from Sigma Aldrich were used. The pH tester was calibrated with standard buffer solutions before measurement. The specifications of the pH testing system used to acquire reference values includes range of 0.00 to 14.00 pH with resolution of 0.01 pH and accuracy of ±0.05 pH. Further, the system has an automatic temperature compensation by using an inbuilt temperature sensor with resolution and accuracy of 0.1°C and ±0.5°C respectively. The electrochemical characterization of pH sensor was

analyzed with cyclic voltammetry (CV), electrochemical impedance spectroscopy (EIS) and potentiometric methods in a two-electrode (SE and RE) system with Autolab electrochemical workstation (PGSTAT302N, Metrohm, Netherland). The CV analyses were carried out at scan rate of 100 mV/s in the potential range of -1 to 1 V. EIS analysis was carried out in a frequency range of 10 Hz to 1 MHz with an amplitude of 10 mV. To test the electrochemical performance of the sensor under the influence of ions and analytes including Na^+, K^+ and glucose which can be widely found in sweat (as shown in Table 1), we prepared dissolved salt solutions of 100 mM NaCl, 100 mM KCl and 100 mM glucose. To further investigate the influence of NaCl on SE's property, we prepared three set of NaCl concentration (1 mM, 10 mM and 100 mM). To test the robustness of fabricated stretchable sensor, the patch was tested with a controlled uniaxial stretch test setup. This stretch test setup has two stepper motors (Micronix, USA) which can stretch the sample from the two sides. For stretchability test of the sensors presented here, the stepper motor was moving at 0.5 mm/s. The resistance between the graphite-polyurethane composite electrode and stretchable interconnect was monitored through a multi-meter (34461A, Agilent).

3. Results and discussion

3.1. pH sensor characterization

The electrochemical reaction at the surface of SE was measured using CV analysis at a scan rate of 100 mV/s. The CV curve of SE in a buffer solution of pH value 7 (Fig. 3(a)) shows that there is no redox or oxidation reaction between active electrode and the solution. The results from CV analysis (Fig. 3(a)) predict non-Faradaic electrochemical reaction and indicate an ideal CV scan for a graphite based electrode. The stability of the SE's electrochemical reaction was tested with 50 cycles CV scan. As presented in Fig. S4, the CV curve during 50 cycles test remains the same shape. As per general mechanism, when the SE reacts with the solution, an electrical double layer (EDL) structure is formed on the surface of the electrode by adsorption of ions. This is due to non-Faradaic electrochemical reaction between graphite composite based electrode and the solution. Variations in the pH value of the test solution leads to changes in the electrical properties such as impedance, capacitance or potential of the EDL by protonation and deprotonation of sensitive electrode (Arshak *et al.,* 2007; Gill *et al.,* 2009;

Manjakkal *et al.*, 2015). These parameters were investigated using EIS and potentiometric analysis as they determine the sensitivity and the sensing mechanism of electrochemical pH sensor. The variation in impedance and capacitance of the EDL depends on the nature of the electrode material and the ionic exchange reaction at the electrode-pH solution interface (Arshak *et al.,* 2007; Gill *et al.,* 2009; Manjakkal *et al.*, 2015). The changes in pH value of the solution lead to variations in the solution resistance (R_{ser}), charge transfer resistance (R_{ct}), double layer capacitance (C_{dl}) and ionic exchange resistance at the electrode-solution interface. The variation of these parameters can be measured by using complex impedance data of the EIS analysis. These parameters were optimized by measuring the variations in the impedance and capacitance values with pH value of solution. However, with reference to readout electronics, the sensitivity is explained in terms of the potential difference between SE and RE. The potentiometric readout is advantageous as it simplifies the circuit design.

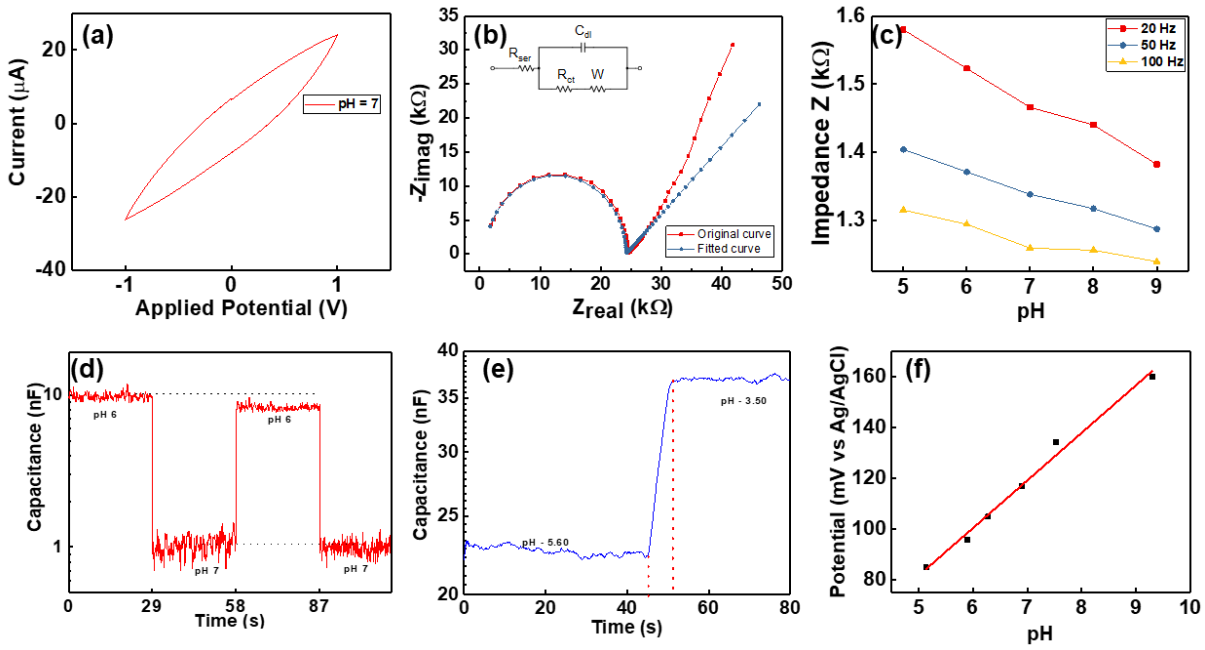

Fig. 3. (a) CV curve and (b) Nyquist plot for graphite-polyurethane composite electrode at pH 7 buffer solution and fitted curve based on Randles circuit model (c) impedance versus pH measured between SE and RE at selected frequencies (d) hysteresis in pH response and (e) response time of the sensor (f) potentiometric performance of the pH sensor.

The complex impedance data of the sensor was analyzed by using Nyquist plot (Fig. 3(b)), which shows a straight line in the lower frequency section and a semicircle is in the higher frequency

range. A similar Nyquist plot can be found for graphite-polyurethane composite in ion detection (Cesarino *et al.*, 2010). The straight line could be attributed to the diffusion of H^+/OH^- ions from the solution into graphite electrode. The impedance due to diffusion of ions also depends on the structural properties of the material. The film shows a rough surface morphology of graphite-polyurethane, as shown in SEM image (SEM S4700, Hitachi) in Fig. S5. For an ideal capacitor, allowing perfect ion diffusion of electrode, the angle of this curve should be 45º. However, our experimental results indicate of about 32º, at a neutral pH value. This indicates a capacitive reactance behavior due to material structure and less ionic concentration at the neutral solution. The Nyquist plot was analyzed using Autolab NOVA software (Metrohm, Netherland). The measured curve was fitted by using the Randles circuit model, which consists of equivalent R_{ser}, C_{dl}, R_{ct} and Warburg diffusion element (W). The fitted Nyquist curve matches the measured curve perfectly in high frequency range. The value of R_{ct}, which is reflected by the diameter of semi-circle, was estimated to be 23.2 kΩ. The charge transfer resistance is related to solution/electrode interaction and transfer of electrons from the SE to external conducting electrode. Some offset in the low frequency range can be observed. This is due to the low diffusion resistance of pH SE. It can indicate a capacitive reactance behavior due to material structure and less ionic concentration at the neutral solution. The steep line observed in the low frequency region of the Nyquist curve also proves a double layer capacitive behaviour. The EIS analysis (Fig. 3(b)(c)) shows that the variations in solution pH changes the electrical properties of EDL and as a result the impedance of SE varies.

The SE electrode was further characterized in DMEM solution, which is a medium used as a blood equivalent solution to check the pH value of a body fluid. This solution offers minimized ion reaction property, which prevents the pH drifting in the solution when diluted HCl/KOH is added for different pH measurement, especially in the range 5-9. Fig. 3(c) exhibits the impedance variation of DMEM solutions at different pH values. A similar observation is found for variations in capacitance at various pH values. The sensor shows a sensitivity of 49 Ω/pH at 20 Hz sweeping frequency. The hysteresis effect of pH sensor was investigated by continuously monitoring its electrical response in terms of capacitance while alternating the pH of the solution between 6 and 7 as shown in Fig. 3(d). The deviation of pH sensor's capacitance at same pH is not significant. The curve indicates a fast and

uniform recovery after every cycle. We estimated the response time by altering the pH in the solution and the pH sensor exhibits a fast response with a response time of 8 s as shown in Fig. 3(e). The response time of the sensor is attributed by many factors including the material, fabrication process and the surface morphology (Lakard *et al.*, 2007). The obtained response time is comparable with the reported metal oxide based pH sensors (Table. S1). In general, one of the major issues in thick-film sensors is their high potential to be interfered by other ions or analytes in the solution. As shown in Table 1, sweat contains glucose in the range of 0.33-0.65 mM, Na^+ 66.3±46.0 mM and K^+ 9.0±4.8 mM. To test the interference effect of the pH sensor with a distinguishable electrical response, the ions and analytes are used here in much higher concentration (100 mM). The influence from Na^+, K^+ ions and glucose on the pH sensor is estimated by monitoring the capacitance of the sensor due to change in the conductivity of solution by adding salts of Na^+ and K^+. The capacitance at 50 Hz is compared between Na^+, K^+ ions and glucose dissolved solution with reference solution (pH 7 buffer solution), as shown in Fig. S6. The relative change in the capacitance are -0.32 for Na^+, -0.28 for Na^+ and K^+ and -0.29 for Na^+, K^+ and glucose. A comparatively higher change in capacitance is observed for Na^+, which could be attributed to the conductivity of solution. To confirm this, a further CV analysis was carried out by varying NaCl concentration between 1 mM, 10 mM and 100 mM, as presented in Fig. S7. CV curve indicates a similar trend for 1 mM and 10 mM NaCl solution. However, a shift in current can be observed at ±1 V potential for 100 mM NaCl solution. In addition, no redox or oxidation reaction is observed between SE and the solution. Hence, it can be concluded that major ions and glucose in sweat will have minor influence on the performance of the fabricated pH sensor.

To transmit pH data in a straightforward way, we also carried out the potentiometric analysis. The measured potential difference (emf- electro motive force) between SE and RE is show in Fig 3(f). We observed a sub-Nernstian response with a sensitivity of 13.76±5.45 mV/pH (n=4) in the range of pH 5-9.5 at room temperature.

3.2. Characterization of pH sensor under stretch conditions

To test the performance of pH sensor under stretching conditions, the resistance between the SE and stretchable interconnect is measured with the experiment setup shown in Fig. 4(a). The original

distance between one end of interconnect and graphite-polyurethane composite electrode is 15 mm. The maximum extension distance from one side of stepper motor is 8 mm, which corresponds to 53% uniaxial strain. At this strain, the resistance variation is 5.6%, as shown in Fig. 4(b). This resistance variation can be attributed to: (i) the deformation in conductors; (ii) change in contact resistance between the graphite-polyurethane composite and stretchable interconnects; and, (iii) change in surface area of micro-structured graphite-polyurethane composite electrode during bending. To evaluate the robustness of pH sensor, further cyclic stretching test was carried out. The sensor was tested up to 500 cycles under 30% strain and the electrical response was found to be stable (Fig. 4(c) and Supplementary Video 1). By comparing the resistance between first cycle of stretch and 500th cycle (Fig. 4(d)), the variation in resistance increases from about 1% after first cycle to about 6% after 500th cycle.

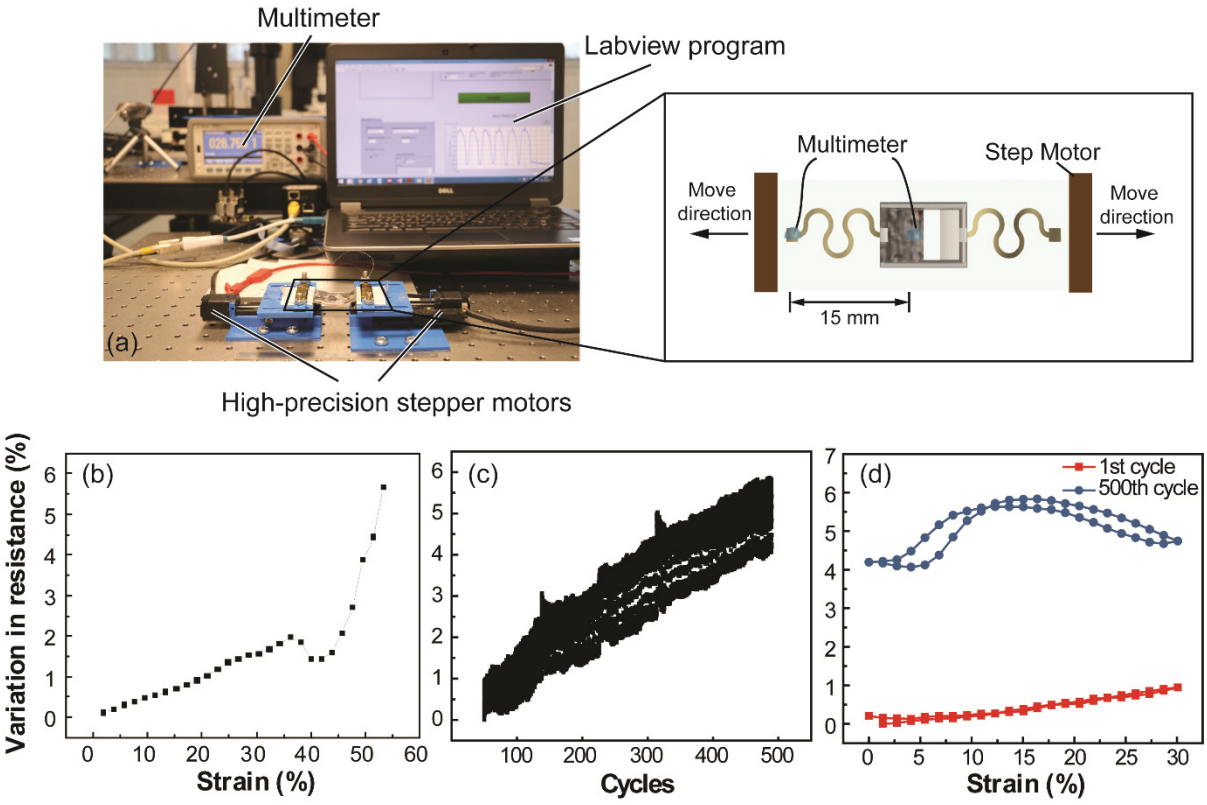

Fig. 4. (a) The electro-mechanical characterization setup controlled with custom LabVIEW program. The inset shows the birds-eye-view of stretchable pH sensor mounted on the setup. (b) The variation in resistance across pH sensing electrode and stretchable interconnect with respect to the external strain experienced by the pH sensor. (c) Cyclic stretching test for stretchable pH sensor up to 30% strain. (d) Comparison in resistance variation between the first cycle of stretching and releasing and 500th cycle.

3.3. Stretchable antenna characterization

The response of stretchable antenna was evaluated through a vector network analyzer (VNA) (Agilent E8362B). This included performance evaluation during stretching. The S-parameter was measured with a frequency range between 10 MHz to 40 MHz. This parameter represents the power reflected through the antenna. From measurement results (Fig. S8) it was observed that the S11 of antenna is reduced by - 1.3dB at 13.56 MHz after tuning with circuit. No shift or distortion was observed in the S-parameter curves for 20% stretched condition. This indicates a stable signal radiation performance of stretchable antenna.

3.4. Evaluation of full system

The real-time wireless pH measurement capability of the developed stretchable sensing system was evaluates as shown in Fig. 5 and Supplementary video 2. A custom smartphone App "SenseAble" was developed with two options for pH data display (Fig. 5(a)). The first option allows display of pH value calibrated on the basis of potentiometric measurement. The second option displays the potential between SE and RE. The temperature from human skin can also be measured as the third option. Considering the influence of temperature on pH sensitivity, the App allows the user to re-calibrate the pH data based on the temperature change. In addition, the App allows users to track the sweat pH with the data storage function as shown in Supplementary video 3. To validate the full system, the fabricated pH sensor was evaluated with a solution equivalent of human sweat. The pH value was wirelessly transmitted to the App as shown in Fig. 5(b). The sensitivity of the pH sensor with solution equivalent of human sweat is about 11.13±5.8 mV/pH (n=3), which is slightly less compared to the sensitivity with DMEM solution. Unlike DMEM solution, the solution equivalent of sweat contains excess ions when the pH is varied. The slight variation in the pH value could be attributed to the excess ions affecting the stability of the solution. The ion reaction disturbs the stability of the solution and leads to pH drifting. In this study, we have assumed that sufficient amount of sweat is available for in-situ analysis. Typically, >10μL of sweat is needed for in-situ analysis (Emaminejad *et al.,* 2017). However, in the case of individuals having sedentary lifestyle, even this amount may not be available. Clinical methods such as 'Iontophoresis' could be used in such cases to extract the sweat on-demand (Leboulanger *et al.*,

2004; Potts *et al*., 2002). The technique has been used by Emaminejad *et al.* for monitoring of Na^+ and Cl^- in sweat and by GlucoWatch by Animas technologies.

Key Features	
pH range	5-9
Sensitivity	11.13 mV/pH
Response time	< 8 s
Stretchability	53% 500cycles@30%
Data transmission	Stretchable antenna
Communication distance	2-3 cm

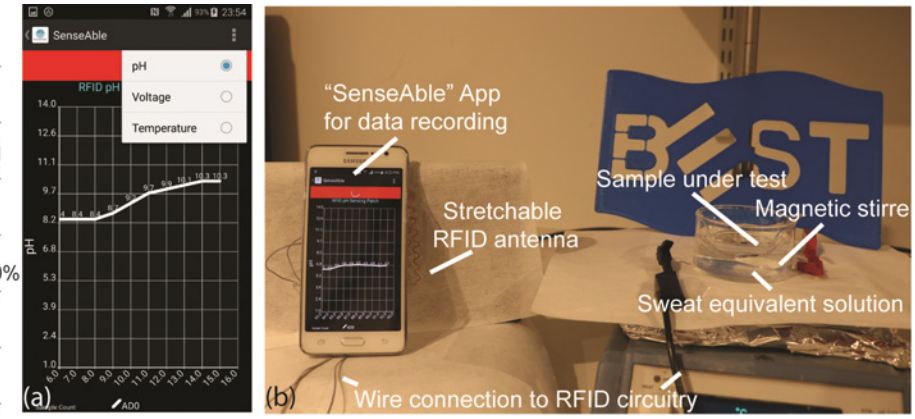

Fig. 5. (a) Screenshot of smartphone App "SenseAble" and (b) photo of real-time pH monitoring system including stretchable pH sensor in sweat equivalent solution, stretchable antenna and mobile monitoring App.

4. Conclusion

In this work, we presented a stretchable system for wireless monitoring of pH from sweat. The pH sensor is based on a novel combination of graphite-polyurethane composite material. An extensive electro-chemical study performed to characterize the pH sensor shows the sensor response in the pH range of 5-9. The pH sensitivity of the fabricated stretchable sensor tested on the human sweat equivalent solution is 11.13±5.8 mV/pH. The interference by major ions and glucose in sweat are negligible. The pH sensing patch with integrated stretchable interconnects is robust with stretching up to 53% strain and more than 500 cycles for 30% strain. The stretchable RFID antenna allows the pH data to be read out without external power through a custom-developed smartphone App. The stretchability also leads to improved conformability of pH sensor system. Compared with the reported wearable pH sensing devices, our stretchable system is advantageous in being highly stretchable and conformable to skin, while offering faster pH sensing response and convenience in terms of wireless data transmission. The costliest component in the developed system is the RF430FRL152H NFC microcontroller IC including which the system could be made less than ~$3.5. The sensor can be disposed-off separately or the entire system could be disposed. Further, the use of low-power

microcontroller helps in local computations for carrying out advanced digital signal processing, multi-sensor calibration routines, flexibility and reconfigurability before transmitting the data to the mobile phone. This feature is not available in other implemented systems reported in literature. The above research could be extended in the in several directions such as detection of multi-biomarkers' including glucose, ammonia and urea with integrated wearable system, smart disposable bandage for wound exudate monitoring, multi-biofluidic solutions forming a body area network.

Acknowledgements

The authors are thankful to James Watt Nanofabrication Centre (JWNC) and Electronic Systems Design Centre (ESDC) at University of Glasgow for support related to fabrication and characterization of the prototype devices. This work was supported in part by the European Commission under grant agreement PITN-GA-2012-317488-CONTEST and EPSRC Fellowship for Growth–Printable Tactile Skin (EP/M002527/1).

Reference

Anastasova, S., Crewther, B., Bembnowicz, P., Curto, V., Ip, H.M.D., Rosa, B., Yang, G.-Z., 2017. Biosens. Bioelectron. 93, 139-145.
Arshak, K., Gill, E., Arshak, A., Korostynska, O., 2007. Sensor. Actuat. B-Chem. 127 (1), 42-53.
Baccarin, M., Cervini, P., Cavalheiro, E.T.G., 2018. Talanta 178, 1024–1032.
Bandodkar, A.J., Hung, V.W.S., Jia, W., Valdes-Ramirez, G., Windmiller, J.R., Martinez, A.G., Ramirez, J., Chan, G., Kerman, K., Wang, J., 2013. Analyst 138 (1), 123-128.
Cesarino, I., Cavalheiro, É.T.G., Brett, C.M.A., 2010. Microchimi. Acta 171(1-2), 1-9.
Corrie, S.R., Coffey, J.W., Islam, J., Markey, K.A., Kendall, M.A.F., 2015. Analyst 140 (13), 4350-4364.
Curto, V.F., Fay, C., Coyle, S., Byrne, R., O'Toole, C., Barry, C., Hughes, S., Moyna, N., Diamond, D., Benito-Lopez, F., 2012. Sensor. Actuat. B-Chem. 171-172, 1327-1334.
Czarnowski, D., Gorski, J., 1991. J. Appl. Physiol. 70 (1), 371-374.
Dahiya, R., 2015. Epidermal electronics: flexible electronics for biomedical applications, in: Carrara, S., Iniewski, K. (Eds.), Handbook of Bioelectronics: Directly Interfacing Electronics and Biological Systems, Cambridge University Press, Cambridge, pp. 245-255.
de Toledo, R.A., Santos, M.C., Cavalheiro, E.T.G., Mazo, L.H., 2005. Anal. Bioanal. Chem. 381 (6), 1161-1166.
Emaminejad, S., Gao, W., Wu, E., Davies, Z.A., Yin Yin Nyein, H., Challa, S., Ryan, S.P., Fahad, H.M., Chen, K., Shahpar, Z., Talebi, S., Milla, C., Javey, A., Davis, R.W., 2017. Proc. Natl. Acad. Sci., 114 (18), 4625-4630.
Farandos, N.M., Yetisen, A.K., Monteiro, M.J., Lowe, C.R., Yun, S.H., 2015. Adv. Healthc. Mater. 4 (6), 792-810.
Gao, W., Emaminejad, S., Nyein, H.Y.Y., Challa, S., Chen, K., Peck, A., Fahad, H.M., Ota, H., Shiraki, H., Kiriya, D., Lien, D.-H., Brooks, G.A., Davis, R.W., Javey, A., 2016. Nature 529 (7587), 509-514.
Gill, E.I., Arshak, A., Arshak, K., Korostynska, O., 2009. IEEE Sens. J. 9 (5), 555-562.
Haghi, M., Thurow, K., Stoll, R., 2017. Healthc. Inform. Res. 23 (1), 4-15.
Heikenfeld, J., 2014. IEEE Spectrum 51 (11), 46-63.

Huang, X., Liu, Y., Chen, K., Shin, W.-J., Lu, C.-J., Kong, G.-W., Patnaik, D., Lee, S.-H., Cortes, J.F., Rogers, J.A., 2014. Small 10 (15), 3083-3090.
Imani, S., Bandodkar, A.J., Mohan, A.M.V., Kumar, R., Yu, S., Wang, J., Mercier, P.P., 2016. Nat. Commun. 7, 11650.
World Heath Organization, 2011. mHealth: New horizons for health through mobile technologies, in Global Observatory for eHealth series (Vol.3), ISBN 978 92 4 1564250. Retrieved from http://www.who.int/goe/publications/goe_mhealth_web.pdf
Kim, J., Banks, A., Cheng, H., Xie, Z., Xu, S., Jang, K.-I., Lee, J.W., Liu, Z., Gutruf, P., Huang, X., Wei, P., Liu, F., Li, K., Dalal, M., Ghaffari, R., Feng, X., Huang, Y., Gupta, S., Paik, U., Rogers, J.A., 2015. Small 11 (8), 906-912.
Lakard, B., Segut, O., Lakard, S., Herlem, G., Gharbi, T., 2007. Sensor. Actuat. B-Chem. 122 (1), 101-108.
Leboulanger, B., Guy, R.H., Delgado-Charro, M.B., 2004. Physiol. Meas. 25 (3), R35-R50.
Lee, H., Song, C., Hong, Y.S., Kim, M.S., Cho, H.R., Kang, T., Shin, K., Choi, S.H., Hyeon, T., Kim, D.-H., 2017. Sci. Adv. 3 (3), e1601314.
Liu, G., Ho, C., Slappey, N., Zhou, Z., Snelgrove, S.E., Brown, M., Grabinski, A., Guo, X., Chen, Y., Miller, K., Edwards, J., Kaya, T., 2016. Sensor. Actuat. B-Chem. 227, 35-42.
Liu, Y., Pharr, M., Salvatore, G.A., 2017. ACS Nano 11 (10), 9614-9635.
Manjakkal, L., Cvejin, K., Kulawik, J., Zaraska, K., Szwagierczak, D., Socha, R.P., 2014. Sensor. Actuat. B-Chem. 204, 57-67.
Manjakkal, L., Djurdjic, E., Cvejin, K., Kulawik, J., Zaraska, K., Szwagierczak, D., 2015. Electrochim. Acta 168, 246-255.
Matsuhisa, N., Kaltenbrunner, M., Yokota, T., Jinno, H., Kuribara, K., Sekitani, T., Someya, T., 2015. Nat. Commun. 6, 7461.
Mohan, S.S., Hershenson, M.d.M., Boyd, S.P., Lee, T.H., 1999. IEEE J. Solid-St. Circ. 34 (10), 1419-1424.
Nakata, S., Arie, T., Akita, S., Takei, K., 2017. ACS Sensor. 2 (3), 443-448.
Nikolajek, W.P., Emrich, H.M., 1976. Klin. Wschr. 54 (6), 287-288.
Garcia Núñez, C., Navaraj, W.T., Polat, E.O., Dahiya, R., 2017. Adv. Funct. Mater. 27 (18), 1606287.
Gupta, S., Navaraj, W.T., Lorenzelli, L., and Dahiya, R., 2018. NPJ Flex. Electron. (in press).
Patterson, M.J., Galloway, S.D.R., Nimmo, M.A., 2000. Exp. Physiol. 85 (6), 869-875.
Potts, R.O., A. Tamada, J., J. Tierney, M., 2002. Diabetes. Metab. Res. Rev., 18, S49-S53.
Quesada-González, D., Merkoçi, A., 2017. Biosens. Bioelectron. 92, 549-562.
Rose, D.P., Ratterman, M.E., Griffin, D.K., Hou, L., Kelley-Loughnane, N., Naik, R.R., Hagen, J.A., Papautsky, I., Heikenfeld, J.C., 2015. IEEE T. Bio-Med. Eng. 62 (6), 1457-1465.
Saciloto, T.R., Cervini, P., Gomes Cavalheiro, É.T., 2013. Anal. Lett. 46 (2), 312-322.
Sakharov, D.A., Shkurnikov, M.U., Vagin, M.Y., Yashina, E.I., Karyakin, A.A., Tonevitsky, A.G., 2010. B. Exp. Biol. Med. 150 (1), 83-85.
Semaan, F.S., Pinto, E.M., Cavalheiro, É.T.G., Brett, C.M.A., 2008. Electroanal. 20 (21), 2287-2293.
Simić, M., Manjakkal, L., Zaraska, K., Stojanović, G.M., Dahiya, R., 2017. IEEE Sens. J. 17 (2), 248-255.
Sonner, Z., Wilder, E., Heikenfeld, J., Kasting, G., Beyette, F., Swaile, D., Sherman, F., Joyce, J., Hagen, J., Kelley-Loughnane, N., Naik, R., 2015. Biomicrofluidics 9 (3), 031301.
Takei, K., Honda, W., Harada, S., Arie, T., Akita, S., 2015. Adv. Healthc. Mater. 4 (4), 487-500.
Tinku, S., Collini, C., Lorenzelli, L., Dahiya, R.S., 2014. IEEE Sens. Proc. 2107-2110.